Applied Catalysis B: Environmental 309 (2022) 121247

Contents lists available at ScienceDirect

Applied Catalysis B: Environmental

journal homepage: www.elsevier.com/locate/apcatb

Electrochemical oxidation of glycerol to hydroxypyruvic acid on cobalt (oxy)hydroxide by high-valent cobalt redox centers

Xin Huang [a,b], Yuyang Guo [b], Yu Zou [a,b], Jiang Jiang [a,b,*]

[a] School of Nano-Tech and Nano-Bionics, University of Science and Technology of China, Hefei 230026, China
[b] i-Lab, CAS Key Laboratory of Nano-Bio Interface, Suzhou Institute of Nano-Tech and Nano-Bionics, Chinese Academy of Sciences, Suzhou 215123, China

ARTICLE INFO

Keywords:
Glycerol
Selective oxidation
Hydroxypyruvic acid
High-valent cobalt center
Redox-mediated

ABSTRACT

Transforming glycerol to value-added chemicals by mild electrochemical oxidation on earth-abundant, low-cost transition metal electrocatalysts is both environmentally and economically beneficial. Herein, substoichiometric cobalt (oxy)hydroxide CoO_xH_y has been demonstrated as an effective electrocatalyst for selective glycerol oxidation to hydroxypyruvic acid (HPA), an important chemical intermediate with three carbon atoms bearing three different functional groups. The Faradaic efficiency for HPA production can reach 43.2%, with an average production rate of 679.2 μmol min^{-1} $m_{geo}{}^{-2}$. Through systematic investigation using cyclic voltammetry, step potential electrochemical spectroscopy, and in situ Raman spectroscopy characterizations, we have revealed that the high-valent cobalt center is responsible for the enhanced activity and selectivity, where electrochemically more stable CoO_x exhibits much lower activity and Faradaic efficiency in comparison. This redox-mediated glycerol oxidation mechanism offers a new perspective for future electrocatalyst development toward selective glycerol valorizations.

1. Introduction

Due to ever-increasing concerns over the energy crisis and environmental pollutions, enormous efforts have been devoted into searching and developing sustainable and renewable alternative sources to fossil fuels. Biodiesel produced from renewable sources like animal fats and vegetable oils has emerged as a viable alternative [1]. However, the rapid development of the biodiesel industry has resulted in a large surplus of glycerol (about 0.1 liter glycerol waste was generated for every liter of biodiesel produced), which is projected to reach 4.0 billion liters per year by 2026 [2,3]. Therefore, glycerol valorization into valuable products has drawn great attention as a means to make biodiesel production more economically feasible and environmentally friendly [4–10]. In addition, glycerol oxidation reaction can also serve as an alternative reaction to replace anodic water oxidation reactions, making hydrogen evolution [11,12] or CO_2 reduction [13,14] more energy-efficient.

The electrochemical glycerol oxidation reaction (GOR) driven by renewable energy is a promising way to produce fine chemicals, where valuable C_3 products such as glyceraldehyde (GLAD), glyceric acid (GLA), and dihydroxyacetone (DHA) have been made using noble metal catalysis such as Pt and Au [15,16]. To reduce the operating cost, earth-abundant transition metal-based nanomaterials have been employed as alternative catalysts, given their excellent performance in water splitting and biomass oxidations [17–20]. However, when they are being applied for electrochemical glycerol oxidation, deep oxidation product such as formic acid is most often obtained [21–30]. It is still a great challenge for finding a cost-effective method to achieve electrochemical valorization of glycerol into value-added chemicals. Very recently, Chiang et al. have reported that in neutral to weakly basic borate buffer solutions, selective production of C_3 products such as DHA can be achieved on transition metal oxides electrodes [31,32]. We have also discovered that it is the coordination effect between borate and glycerol, promotes the electrochemical activity of glycerol on transition metal (cobalt or nickel) borate electrodes, and suppresses the undesirable C-C bond cleavage, thus achieving highly selective production of DHA [33]. However, the reported electrochemical glycerol oxidation activity remained limited with selectivity mainly toward DHA; while other valuable C_3 product such as hydroxypyruvic acid (HPA), an important chemical intermediate with three carbon atoms bearing three different functional (hydroxyl, keto, and carboxyl) groups, has not been produced by glycerol oxidation using low cost transition metal catalysts.

* Corresponding author at: School of Nano-Tech and Nano-Bionics, University of Science and Technology of China, Hefei 230026, China.
E-mail address: jjiang2010@sinano.ac.cn (J. Jiang).

https://doi.org/10.1016/j.apcatb.2022.121247
Received 21 December 2021; Received in revised form 17 February 2022; Accepted 21 February 2022
Available online 23 February 2022

High-valent transition metal species (M^{3+} and M^{4+}, M = Co or Ni) has been reported to be actively involved in water oxidation reactions [34–37]. Very recently, these high-valent redox pairs were also found to be critical for simple alcohol and biomass such as hydroxymethylfurfural (HMF) oxidation reactions [38–43]. However, there has been no report on their application in electrochemical glycerol oxidation reaction, likely due to the complicated glycerol oxidation pathways, and undesirable breaking of the C-C bond under commonly used strong alkaline conditions.

Herein, we report efficient electrochemical glycerol oxidation to valuable C_3 products on substoichiometric cobalt (oxy)hydroxide CoO_xH_y electrodes for the first time. Hydroxypyruvic acid, a valuable chemical intermediate, has been produced with high Faradaic efficiency (43.2%). Through systematic investigation using cyclic voltammetry, step potential electrochemical spectroscopy, and in situ Raman spectroscopy, we have correlated the enhanced activity and HPA selectivity to the electrochemically generated high-valent cobalt species rich in CoO_xH_y. Despite CoO_xH_y exhibits a lower electrochemically active surface area compared to spinel cobalt oxide CoO_x which generates DHA as major product, CoO_xH_y displays higher activity and Faradaic efficiency for C_3 products, further demonstrating the important role of high-valent cobalt center in enhancing the activity and affecting the selectivity of electrochemical glycerol oxidation. A tentative indirect oxidation mechanism is proposed, where glycerol is first oxidized to DHA through a $2e^-$ oxidation process mediated by Co^{3+}/Co^{4+} redox pairs, and then DHA undergoes subsequent $4e^-$ oxidation to produce HPA by Co^{2+}/Co^{3+} redox mediators.

2. Experimental section

2.1. Materials

Glycerol ($C_3H_8O_3$, 99%), dihydroxyacetone ($C_3H_6O_3$, 99%), cobalt nitrate hexahydrate ($Co(NO_3)_2{\cdot}6H_2O$, 98.5%), potassium nitrate (KNO_3, 99%), sulfuric acid (H_2SO_4, 98%), sodium tetraborate decahydrate ($Na_2B_4O_7{\cdot}10H_2O$, 99.5%), and boric acid (H_3BO_3, 99.8%) were purchased from Sinopharm Chemical Reagent Co., Ltd. All chemicals were used as received without further purifications. Deionized water (Millipore, Milli-Q grade) was used in all experiments. Carbon fiber cloth (CF) was obtained from Shanghai Hesen Electric Co., Ltd, and cut into pieces of 1.5 × 3 cm^2 for later use.

2.2. Fabrication of CoO_xH_y/CF and CoO_x/CF electrodes

The CoO_xH_y electrode was prepared by a one-step electrodeposition process on carbon fiber cloth (CF). Before its usage, the CF substrate was ultrasonically washed with acetone, ethanol, and finally deionized water for 30 min each, and then dried at 50 °C under ambient atmosphere. After that, the CoO_xH_y nanoarrays were deposited onto the surface of carbon fiber cloth via electrodeposition, using a three-electrode configuration (carbon fiber cloth, Pt sheet, and Ag/AgCl were applied as the working electrode, the counter electrode, and the reference electrode, respectively) on a CHI660E electrochemical workstation (ChenHua Co. Ltd., Shanghai). The electrodeposition of CoO_xH_y was conducted at − 0.85 V vs. Ag/AgCl (sat. KCl) in 0.1 M KNO_3 solution containing 10 mM $Co(NO_3)_2{\cdot}6H_2O$ at room temperature for 600 s. After the electrodeposition, that carbon fiber cloth was taken out and cleaned carefully with deionized water several times, then dried at 50 °C for further usage.

For CoO_x/CF electrode preparation, the as-prepared CoO_xH_y/CF electrode was thermally heated to and maintained at 400 °C in a furnace under N_2 protection for 2 h, and then cooled down naturally for further usage.

2.3. Sample characterization

Sample morphologies were acquired and investigated under scanning electron microscope (SEM, JEOL JSM-7500F, Japan) and transmission electron microscope (TEM, JEOL JEM-2100F, 600 kV). To perform the TEM experiment, the samples were detached from CF substrate, dispersed in ethanol by ultrasonic treatment for 30 min, and then deposited on the copper grid. Sample surface composition and valence states were surveyed and analyzed by powder X-ray diffraction (XRD, RIGAKU D/Max 2500 diffractometer using Cu Kα radiation, 40 kV and 40 mA), X-ray photoelectron spectroscopy (XPS, XASAM 800, Kratos Analysis, U.K.) with an Al Ka X-ray source (1486.6 eV) and a beam size of ~1 mm. Raman spectra were acquired on a Renishaw Raman InVia equipped with a CCD detector and coupled to a Leica microscope that allows a rapid acquisition of Raman spectra with a spatial resolution of about 1 μm (micro-Raman technique). The excitation wavelength was 785 nm, and a 50 × objective with a numerical aperture of 0.50 was used. Solution pH were measured by LeiCi-PHS-3C pH meter (Shanghai Precision & Scientific Instrument Co., Ltd.).

2.4. Electrochemical measurements

All experiments were performed on a CHI660E electrochemical workstation. The electrochemical cell was set up in a typical three-electrodes configuration, with the CoO_xH_y/CF or CoO_x/CF as the work electrode, a platinum foil (1 cm^2) as the counter electrode, and Ag/AgCl (Sat. KCl) as the reference electrode ($E_{Ag/AgCl}$ = 0.197 V vs. SHE). The electrolyte solution was 0.1 M borate buffer solution with a solution pH of 7.52 by mixing 80% 0.4 M H_3BO_3 with 20% 0.1 M $Na_2B_4O_7$ aqueous solution.

For electrochemical measurements, the cyclic voltammogram curves of the CoO_xH_y and CoO_x working electrodes were both acquired at a scan rate of 1 mV s^{-1}. Electrochemical active surface area (ECSA) was inferred from the electrochemical double-layer capacitances (C_{dl}) of the samples, which were determined by performing cyclic voltammetry (CV) in the potential region with no Faradaic processes at different scan rates (1, 2, 4, 6, 8, and 10 mV s^{-1}). The average capacitive currents measured in the middle of the potential range were plotted as a function of the potential sweep rates. The ECSA is calculated based on the following equation:

$$C_{dl} = \frac{|j_a - j_c|}{2v} \quad (1)$$

$$ECSA = \frac{C_{dl}}{A \times C_s} \quad (2)$$

Where the j_a and j_c are the anodic and cathodic current densities, respectively, and v is the scan rate, C_{dl} is the measured double-layer capacitances, A is the geometry area of catalysts (1.5 cm^2), C_s is the specific capacitance, which is set as 80 μF cm^2 here.

For product collection, chronoamperometry testing was conducted using an H-type cell containing 20 mL of electrolyte in each compartment. After the accumulated charges reached a certain level, the electrolyte solution was collected and diluted, by mixing 1 mL of electrolyte with 0.5 mL of 0.1 M H_2SO_4.

All the electrochemical data were displayed without iR compensation, and the potentials were referenced to reversible hydrogen electrode (RHE) according to the following equation:

$$E_{RHE} = E_{Ag/AgCl} + 0.059 \times pH + 0.197 \quad (3)$$

2.5. Product quantification

The concentrations of the reactants and oxidation products were determined by high performance liquid chromatography (HPLC, Ultimate 3000, Thermo Fisher Scientific) equipped with a multiple

wavelength detector (MWD), using a ChromCore Sugar-10H column (Nano Chrom Technologies Co., Ltd. Suzhou) and an ultraviolet-visible detector set at 210 nm for products analysis. For sample separation, column temperature was set at 65 °C with 5 mM H_2SO_4 aqueous solution as the eluent. The flow rate was 0.5 mL min^{-1}, and the injection volume was 20 μL. For each product, calibration curves were obtained using a known concentration of various compounds, ranging from 0 to 50 mg L^{-1} which were provided in our previous report [33].

Faradaic efficiency (FE) of the electrochemical glycerol ($C_3H_8O_3$) oxidation was calculated based on the following balanced half-reactions, corresponding to the conversion of glycerol into individual oxidized C_3 (GLAD: glyceraldehyde, DHA: dihydroxyacetone, GLA: glyceric acid, HPA: hydroxypyruvic acid), C_2 (glycolic acid: GA), and C_1 (formic acid: FA) products.

$$C_3H_8O_3 + 2OH^- \rightarrow C_3H_6O_3(GLAD \quad or \quad DHA) + 2H_2O + 2e^- \tag{4}$$

$$C_3H_8O_3 + 5OH^- \rightarrow C_3H_5O_4^-(GLA) + 4H_2O + 4e^- \tag{5}$$

$$C_3H_8O_3 + 7OH^- \rightarrow C_3H_3O_4^-(HPA) + 6H_2O + 6e^- \tag{6}$$

$$C_3H_8O_3 + \frac{13}{2}OH^- \rightarrow \frac{3}{2}C_2H_3O_3^-(GA) + 5H_2O + 5e^- \tag{7}$$

$$C_3H_8O_3 + 11OH^- \rightarrow 3HCOO^-(FA) + 8H_2O + 8e^- \tag{8}$$

The overall Faradaic efficiency (FE) toward all value-added products is calculated based on the following equation:

$$FE_{product} = \frac{N_{product} \times C_{product} \times V \times F}{Q_{total}} \times 100\% \tag{9}$$

where $N_{product}$ is the number of required charges to oxidize glycerol molecule toward the specific product molecule; $C_{product}$ is the product concentration (mol L^{-1}); V is the volume of the electrolyte solution (2×10^{-2} L); F is Faraday's constant (96,485 C mol^{-1}); Q_{total} is the total charge (C) passed during the electrocatalytic reaction.

The production rate of liquid products was calculated based on the following equation:

$$Production \quad rate = \frac{n_{product}}{A_{cat} \times t} \tag{10}$$

in which $n_{product}$ was the amount of collected product, A_{cat} was the geometric area of the catalyst (1.5 cm^2), and t was the duration of GOR.

Glycerol conversion was inferred indirectly by calculating all the detected solution products of GOR, based on the following equation:

$$Conversion = \frac{Total \ \ carbon \ \ in \ \ product}{Total \ \ carbon \ \ in \ \ glycerol} = \frac{3 \times n_{HPA} + 3 \times n_{GLA} + 3 \times n_{GLAD} + 2 \times n_{GA} + 3 \times n_{DHA} + n_{FA}}{3 \times n_{GLY}} \tag{11}$$

where n_{DHA}, n_{GLAD}, n_{GLA}, n_{GA}, n_{HPA}, and n_{FA} are the detected amount (mmol) of respective oxidation products.

3. Result and discussion

3.1. Electrocatalysts preparation and characterizations

Substoichiometric cobalt (oxy)hydroxide CoO_xH_y was electrodeposited on carbon cloth using cobalt nitrate as precursor, following published protocols with slight modifications [44]. The electrodeposited CoO_xH_y was in the form of nanoarray structures, as shown in its scanning electron microscopy (SEM) image (Fig. 1a). The as prepared CoO_xH_y appeared to be in poor crystallinity, indicated by its high-resolution transmission electron microscopy (HRTEM) image (Fig. 1b), and the corresponding selected area electron diffraction patterns (SAED, Fig. 1b inset). In addition, the X-ray diffraction (XRD) pattern acquired on CoO_xH_y shows no apparent diffraction peaks (Fig. S1), further indicates its poor crystalline form.

Raman scattering spectra can often provide detailed information on the identity of metal oxides and metal (oxy)hydroxides. Therefore, Raman spectra of the as-prepared CoO_xH_y was acquired and shown in Fig. 2a. Two broad spectral features appeared at around 498 and 591 cm^{-1} in its Raman spectrum, which is commonly attributed to the E_g lattice vibrational mode of CoOOH and $A_{2\,u}$ lattice vibrational mode of $Co(OH)_2$ respectively [45,46], indicating the as-prepared CoO_xH_y sample contained a portion of cobalt (oxy)hydroxide CoOOH on the surface as a result of oxidation from $Co(OH)_2$. Furthermore, the oxidation states of Co in the as-prepared samples were investigated and analyzed by X-ray photoelectron spectroscopy (XPS). The complete survey spectrum of the as-prepared CoO_xH_y sample is displayed in Fig. 2b, with main peaks indexed to Co 2p, O 1s, and C 1s. In the high-resolution XPS spectrum of Co 2p (Fig. 2c), the Co $2p_{3/2}$ peak was fitted by two peaks at 782.0 and 780.5 eV with a broad satellite peak at 786.0 eV, which were slightly lower in binding energy compared to the literature values reported for $Co(OH)_2$, due to the oxidized surface [45,47]. In addition, the high-resolution XPS spectrum of O 1s (Fig. 2d) shows two deconvoluted peaks appearing at 532.1 and 530.6 eV in the O 1s binding energy region, which correspond to the adsorbed H_2O (H_2O_{ad}) and hydroxyls (O-H) on CoO_xH_y surface, respectively. Both Raman spectra and XPS results suggest amorphous cobalt (oxy)

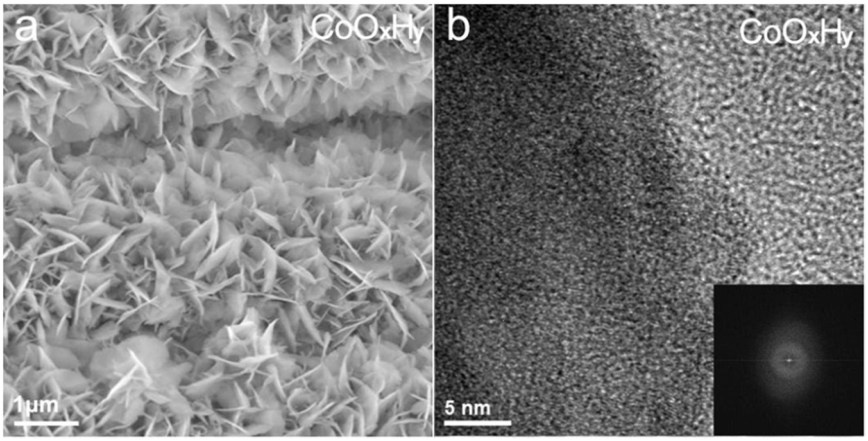

Fig. 1. (a) SEM and (b) HRTEM image of the as-prepared CoO_xH_y, the corresponding selected area electron diffraction (SAED) pattern is shown as inset.

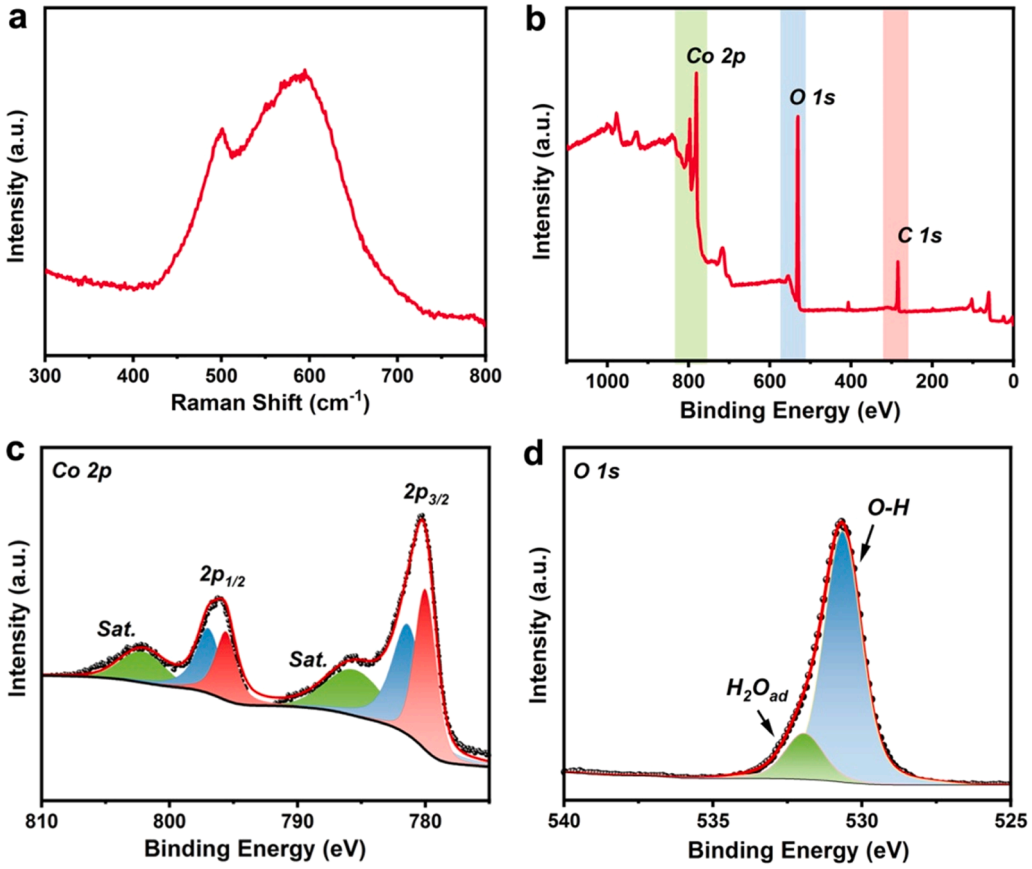

Fig. 2. (a) Raman spectrum, (b) XPS survey spectrum, the high-resolution XPS spectra of Co 2p (c) and O 1s (d) of CoO_xH_y.

hydroxide was successfully synthesized by electrodeposition, in accordance with the TEM and XRD characterization results.

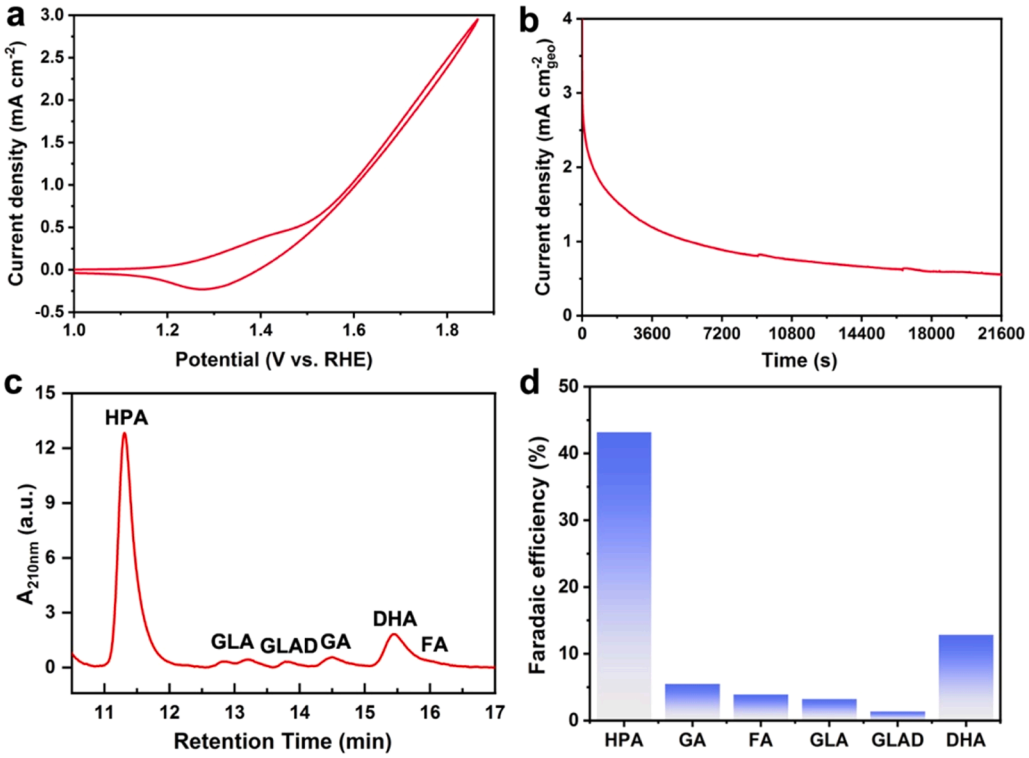

Fig. 3. (a) Cyclic voltammetry conducted in 0.1 M borate buffer solution (pH 7.52) with 0.05 M glycerol, the scan rate was 1 mV s^{-1}. (b) I-t curve of glycerol oxidation at an applied potential of 1.56 V vs. RHE. (c) HPLC chromatogram and (d) the calculated Faradaic efficiencies of various solution oxidation products obtained from electrochemical glycerol oxidation reactions on CoO_xH_y at an applied potential of 1.56 V vs. RHE in 0.1 M borate buffer solution (pH 7.52) containing 0.05 M glycerol, with the accumulated passed charges of 30 C. The applied potentials were displayed without iR compensation for all of the electrochemical measurements reported herein.

3.2. Electrochemical glycerol oxidation on CoO_xH_y electrodes

To investigate the electrochemical glycerol oxidation activity of CoO_xH_y, cyclic voltammograms were first recorded using nanomaterials deposited on carbon fibers as the electrodes. Fig. 3a shows the typical cyclic voltammogram recorded on CoO_xH_y electrode in 0.1 M borate buffer solution (pH 7.52) that contained 0.05 M glycerol, at a scan rate of 1 mV s^{-1}. A pair of redox peaks was observed at 1.41 and 1.26 V during the anodic and cathodic scans, and the current density was seen to increase rapidly from 1.56 V. The redox peaks appeared at 1.41 and 1.26 V correspond to the maximum currents for the oxidation and reduction of Co^{2+}/Co^{3+} redox couple, respectively. The rapidly increasing current density from 1.56 V can be attributed to the glycerol oxidation and possible oxygen evolution on CoO_xH_y surface.

To evaluate the GOR performance on CoO_xH_y more quantitatively, chronoamperometry tests were conducted at a constant potential of 1.56 V (as shown in Fig. 3b). The oxidation products were collected and run through the HPLC column for identification and quantifications when the accumulated passed charges reached 10, 30, and 50 C at 1.56 V. The detailed HPLC chromatograms and the amount of accumulated products were provided in Fig. S2. The representative HPLC chromatogram with the total passed charges of 30 C was shown in Fig. 3c. Similar to our previous results using Co-B_i electrocatalyst [33], six liquid oxidation products were indentified, including glyceraldehyde (GLAD), glyceric acid (GLA), DHA, HPA, glycolic acid (GA), and formic acid (FA). However, the product distribution differed significantly on CoO_xH_y electrodes, which produced a large amount of HPA, besides DHA. The Faradaic efficiencies were calculated to be 43.2%, 5.5%, 3.9%, 3.2%, 1.3%, and 12.8% for HPA, GA, FA, GLA, GLAD, and DHA respectively (Fig. 3d), with the total Faradaic efficiency for C_3 solution products reaching over 60%. The calculated average production rate of HPA is 679.2 μmol min^{-1} $m_{geo}{}^{-2}$, demonstrating efficient electrochemical oxidation of glycerol to HPA using CoO_xH_y as electrocatalyst. Upon further increasing the applied potentials to 1.66 V and 1.76 V, the Faradaic efficiencies for HPA productions decreased to 30.1% and 19.7% together with a clear decline of total solution products FE (Fig. S3), suggesting possible further oxidation of HPA to CO_2 at high anodic potentials on CoO_xH_y surface. In terms of the solution product selectivity, over 80% solution products were C_3 chemicals (4.5% GLA, 3.8% GLAD, 36.1% DHA, and 38.1% HPA), as shown in Fig. S4. The glycerol conversion can be inferred indirectly by calculating all the detected solution products (Fig. S2b) using Eq. (11). For GOR performed on CoO_xH_y at a constant potential of 1.56 V vs. RHE in 0.1 M borate buffer solution (pH 7.52) containing 0.05 M glycerol, the calculated glycerol conversion was 5.1% after 30 C were passed.

In our previous publication, we have assigned HPA as the direct oxidation product of DHA in borate buffer, which was first oxidized from glycerol by $2e^-$ oxidation of the secondary hydroxyl group in glycerol [33]. Therefore, it is reasonable to propose that DHA can be facilely oxidized to HPA on CoO_xH_y surface. To probe and evaluate the oxidation activity of DHA on CoO_xH_y electrodes surface, chronoamperometry measurements were conducted in 0.1 M borate buffer solution (pH 7.52) containing 0.05 M glycerol or 0.05 M DHA, at various applied potentials. Their typical i-t curves were provided in Fig. S5, and the steady-state current density values extracted from the i-t curves at various applied potentials were plotted in Fig. S6, together with the currents obtained in the absence of glycerol and DHA, which served as an indicator of oxygen evolution reaction (OER) activity. The specific current densities followed the order of OER < GOR < DOR (DHA oxidation reaction). The ratio of DOR current to GOR current was over 2 in the test potential window, suggesting that the oxidation of DHA was much more facile than glycerol on the CoO_xH_y electrode. As a result, upon $2e^-$ oxidation of glycerol to DHA, further oxidation of DHA could occur on the CoO_xH_y electrode surface, thus producing large amount of HPA.

3.3. Redox-mediated electrochemical activity on CoO_xH_y

When transition metal (oxy)hydroxides are used as catalysts for electrochemical oxidation reactions, the redox couple such as M^{2+}/M^{3+} and M^{3+}/M^{4+} are often considered as the real active sites. To shed light on the role of high-valent transition metal redox pairs in the electrochemical glycerol oxidation performance on CoO_xH_y, cyclic voltammetry and step potential electrochemical spectroscopy were conducted. Typical cyclic voltammograms recorded on CoO_xH_y under OER, GOR, and DOR conditions at a scan rate of 1 mV s^{-1} are plotted together for comparison in Fig. 4a. Under OER conditions, i.e. in the absence of organic substrate, a pair of redox peaks appeared at 1.41 V and 1.26 V in the anodic and cathodic regions, followed by rapidly increasing current density from 1.66 V (Fig. 4a, black dashed line). These two redox events are generally ascribed to the maximum currents for the oxidation and reduction of the Co^{2+}/Co^{3+} redox couple, respectively. The slowly increasing current density from 1.56 V is assigned to the oxidation of Co^{3+} to Co^{4+}, which was overlapped by the large oxygen evolution current from 1.66 V. The existence of Co^{3+}/Co^{4+} redox couple can be better appreciated by the cyclic voltammogram recorded at faster scan rate, in which a clear reduction peak could be observed at ~1.51 V in the backward scan (E_{pc}' wave in Fig. S7). When glycerol or DHA was present in the electrolyte, due to lower onset oxidation potential of alcohols relative to water, cyclic voltammograms recorded under GOR and DOR conditions show rather inconspicuous Co^{2+}/Co^{3+} and Co^{3+}/Co^{4+} redox peaks (Fig. 4a and Fig. S7). For glycerol oxidation (Fig. 4a, green dotted line), an anodic peak around 1.41 V was still resolvable, followed by rapidly increasing currents from 1.51 V. Under DOR conditions, the anodic current was observed to increase slowly from 1.16 V, with no identifiable Co^{2+}/Co^{3+} redox peak (Fig. 4a, red solid line). In addition, during the backward scan (Fig. S7), the cathodic peak of Co^{3+}/Co^{4+} at 1.51 V which appeared under OER conditions, completely disappeared when glycerol or DHA were present, suggesting the absence of high-valent Co^{4+} ions, possibly due to fast consumption of high-valent Co^{3+} and Co^{4+} species by alcohol molecules.

Oxidation of alcohol and aldehyde by high-valent transition metal ions through a hydrogen atom transfer process has been understood since the 1970 s [48]. Therefore, the disappearance of Co^{3+}/Co^{4+} redox event but not Co^{2+}/Co^{3+} redox couple in the presence of glycerol, suggests that Co^{4+} could induce the dehydrogenation of glycerol, while Co^{3+} could not. In comparison, when DHA was present, other than the disappearance of Co^{3+}/Co^{4+} redox couple, the Co^{2+}/Co^{3+} redox pair was also greatly diminished (Fig. 4a and Fig. S7), indicating complete consumption of Co^{4+} and greatly reduced Co^{3+} concentration by DHA. Similar observation has been reported for simple alcohol or biomass 5-hydroxymethylfurfural (HMF) oxidation reactions on Ni- and Co-based electrocatalysts [38]. The above results suggest that the electrochemically generated Co^{3+} and Co^{4+} play different roles in the glycerol oxidation process, in which Co^{3+} could induce dehydrogenation of DHA, but not glycerol to the same extent, while Co^{4+} displayed much stronger oxidation capability.

Furthermore, we have analyzed the charge/discharge kinetics by performing cyclic voltammetry tests at various scan rates from 1 to 10 mV s^{-1} (Fig. S8). In general, the peak current (I_p) obeys a power law relationship with scan rate ν in the form of $I_p = a\nu^b$, where a and b are fitting parameters [49,50]. When the parameter b is close to 0.5, the current is controlled by semi-infinite linear charge diffusion, indicative of a Faradaic redox process in the bulk; if b is close to 1.0, the current is dominated by a surface-reaction-limited response. By plotting the peak current during the backward scan against ν in a double-logarithmic plot, the b value can be obtained as the slope of linear regression. The calculated values of b for OER, GOR, and DOR reactions on CoO_xH_y were 1.15, 0.84, and 0.68, respectively (Fig. S8). The discharge peak current under OER condition is close to 1, which is indicative of a surface-reaction-limited response, such as charge/discharge of double-layer capacitances. While the value of b decreased to 0.84 and

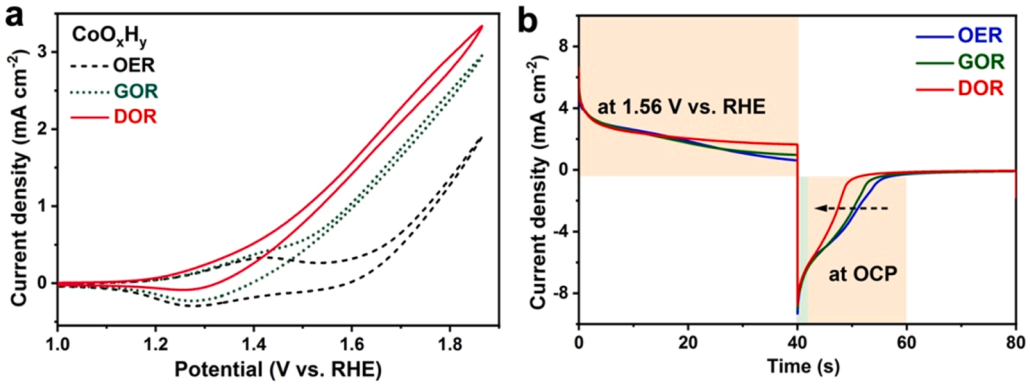

Fig. 4. (a) Cyclic voltammetry performed on CoO_xH_y in 0.1 M borate buffer under OER, GOR, and DOR conditions, with the scan rate of 1 mV s^{-1}. (b) Step potential electrochemical spectroscopy measurements on CoO_xH_y under different conditions.

0.68 under GOR and DOR conditions, approaching the limiting value of 0.5, suggesting more contribution from current that is controlled by semi-infinite linear charge diffusion, i.e. Faradaic redox processes.

Even with very slow scan rate, the capacitive charge storage cannot be completely ruled out easily for nanostructured electrocatalysts. Therefore, the step potential electrochemical spectroscopy (SPECS) experiments were further conducted to separate Faradaic and capacitive charge storage contributions on CoO_xH_y electrodes [51]. Firstly, the open circuit potential (OCP) values of these two electrodes were obtained by performing OCP tests for more than 6 h (Fig. S9). Then, after fresh electrodes were oxidized at 1.56 V for 40 s, the applied potential was jumped to the pre-determined OCP values and held for 40 s while the electrode equilibrated. During this time, the discharging current flow was measured as a function of time. Shown in Fig. 4b, the current decay on CoO_xH_y electrode includes both fast (seconds) and slow (tens of seconds) kinetics, under OER, GOR, and DOR conditions. The fast decay current originates from discharge of the double layer capacitance, while the slower component is due to non-capacitive i.e. redox discharge. Moreover, the passed charges and time required to reach equilibrium follow the order of DOR < GOR < OER, indicating much less redox pairs existed in the presence of DHA, consistent with the cyclic voltammograms shown in Fig. 4a. The above results show that high-valent Co^{3+} and Co^{4+} ions were consumed by the dehydrogenation reaction of glycerol, and in particular DHA.

3.4. *In situ Raman investigation on redox-behaviors of CoO_xH_y*

To corroborate the conclusions drawn from the above cyclic voltammetry and SPECS measurements, we conducted in situ Raman spectroscopy under electrochemical conditions. Fig. 5a shows in situ Raman spectra recorded on CoO_xH_y in pure borate buffer, scanned from open circuit potential (OCP) to 1.66 V with a scan rate of 1 mV s^{-1}. Two

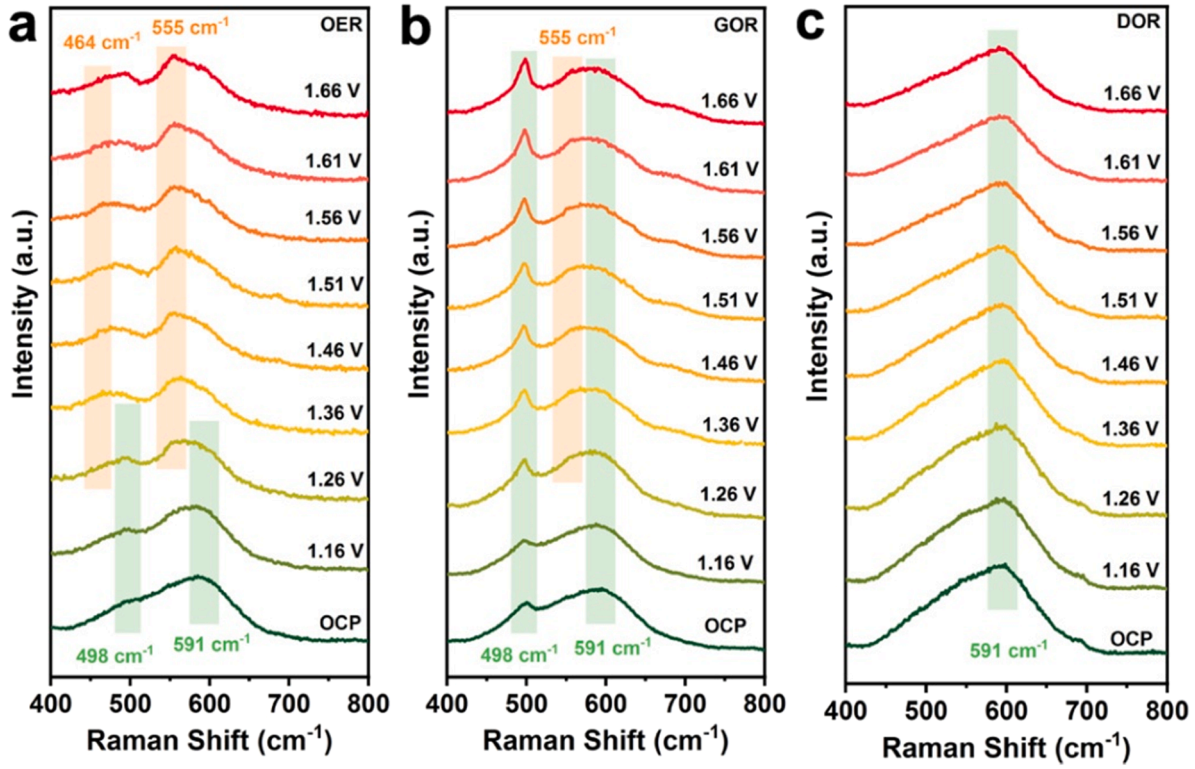

Fig. 5. In situ Raman spectroscopy conducted on CoO_xH_y electrodes at increasing applied potentials from OCP to 1.66 V in 0.1 M borate buffer solution without organic substances (a), or with 0.05 M glycerol (b) or 0.05 M DHA (c).

broad peaks centered at 498 and 591 cm^{-1} were observed at OCP, which can be ascribed to the E_g lattice vibrational mode of CoOOH and $A_{2\,u}$ lattice vibrational mode of $Co(OH)_2$ [36,45,46]. Upon increasing the applied potential to 1.26 V, two new peaks at 464 and 555 cm^{-1} appeared, which could be assigned to the $A_{1\,g}$ and E_g vibrational mode of disordered CoO_2 lattice, respectively [36,38,45,52,53]. This provides strong evidence that CoO_xH_y surface was electrochemically oxidized to generate high-valent Co^{3+} and Co^{4+} ions, with a threshold voltage of 1.26 V under OER condition. When glycerol was added into the electrolyte (0.05 M glycerol in 0.1 M borate buffer), in situ Raman spectroscopy shows that E_g lattice vibrational mode of CoOOH at 498 cm^{-1} gained strength upon increasing the applied potential (Fig. 5b), indicating electrochemical oxidation of CoO_xH_y and the generation of more Co^{3+}. However, the existence of Co^{4+} (555 cm^{-1}) is barely visible. This indicates that Co^{4+} can be consumed by glycerol, but not Co^{3+}. Similar measurements were also conducted in the presence of DHA. As shown in Fig. 5c, the E_g lattice vibrational mode of CoOOH centered at 498 cm^{-1} due to surface oxidation of CoO_xH_y disappeared in DHA solution at OCP, indicating DHA is able to reduce CoOOH back to $Co(OH)_2$. In addition, no significant changes in the Raman spectra of CoO_xH_y were observed even with the applied potential raised to 1.66 V, showing only dominant $A_{2\,u}$ lattice vibrational mode of $Co(OH)_2$ throughout the applied potential window. That is to say, not only Co^{4+} but also Co^{3+} species were difficult to accumulate on CoO_xH_y surface in presence of DHA. The largely suppressed accumulation of Co^{4+} on CoO_xH_y surface under GOR condition and the missing Co^{3+} signal under DOR condition, indicate that the generated Co^{4+} could be rapidly depleted by dehydrogenation of both glycerol and DHA, while the generated Co^{3+} could only be depleted by dehydrogenation of DHA, revealing the distinct roles of electrochemically generated Co^{3+} and Co^{4+} to the oxidation of glycerol and DHA.

Surface oxidation revealed by in situ Raman was also confirmed by ex situ high-resolution XPS spectra of Co 2p, where the Co $2p_{3/2}$ peak of CoO_xH_y were fitted at 779.9 eV and 781.28 eV with a satellite peak fitted at 785.29 eV (Fig. S10a). The Co $2p_{3/2}$ peak appeared to be shifted from 780.5 eV and 782.0 eV of the as-prepared CoO_xH_y (Fig. 2c), indicating that CoO_xH_y underwent irreversible surface oxidation under the GOR process. In addition, the surface oxidation also results in the appearance of lattice oxide ions O^{2-} (O-O) peak at 529.4 eV in the high-resolution XPS spectra of O 1s (Fig. S10b). However, the morphology of CoO_xH_y remained the same after electrocatalytic reactions, as revealed by SEM image (Fig. S10c).

3.5. Comparative studies on CoO_x electrodes

To provide further evidence on the critical role of high-valent cobalt redox centers, we conducted comparative studies on CoO_x electrodes, which are generally stable under electrochemical conditions, as opposed to CoO_xH_y. In order to keep the comparison more valid, we obtained CoO_x by annealing the as prepared CoO_xH_y at 400 °C for 2 h under N_2 protection. After the thermal annealing treatment, the original nanoarray structures of CoO_xH_y were retained, but appeared with a slightly larger size and porous features (Fig. S11a). The HRTEM image (Fig. S11b) and selected area electron diffraction pattern (Fig. S11b inset) show that CoO_x was in good crystalline form. The well-crystallized CoO_x exhibits a clear XRD pattern which can be indexed to the spinel Co_3O_4 phase (JCPDS 42-1467), with characteristic 2-theta peaks at 31.27 (220), 36.85 (311), and 59.3 (511) (Fig. S12). The respective XPS spectra of Co 2p and O 1s are displayed in Fig. S13, with Co $2p_{3/2}$ peak fitted by three peaks at 782.43, 781.13, 779.8 eV and two satellite peaks at 789.43 and 785.43 eV, in good agreement with literature values of Co_3O_4 [45,47]; while O 1s spectrum can be fitted by three deconvoluted peaks at the binding energy values of 533.3, 530.8, and 529.8 eV, which belong to the adsorbed water (H_2O_{ad}), hydroxyls (O-H) on Co_3O_4 surface, and the lattice oxygen in Co_3O_4 (O-O), respectively [35,45].

When CoO_x was used in electrochemical glycerol oxidation reaction, we observe much smaller anodic current density compared to that recorded on CoO_xH_y electrodes. To exclude potential contribution of different active sites density that may exist giving the observed morphological difference between CoO_xH_y and CoO_x, the intrinsic activities to glycerol oxidation were evaluated by normalizing the measured current to their respective electrochemically active surface area (ECSA). As shown in Fig. S14, a double-layer capacitance was determined to be 0.259 mF cm^{-2} for CoO_xH_y, which is more than an order of magnitude smaller than that of CoO_x at 2.91 mF cm^{-2}. The drastic increase of the active surface area of CoO_x compared to CoO_xH_y may be due to the porous structures formed after the thermal annealing process [54]. As a consequence, the specific current density normalized by ECSA on CoO_xH_y (0.17 mA cm_{ECSA}^{-2}) is about 20-fold to that on CoO_x (0.008 mA cm_{ECSA}^{-2}) after 6 h chronoamperometry test (Fig. S15), indicating that the intrinsic electrochemical activities to glycerol oxidation on CoO_xH_y is much higher than its corresponding metal oxides form.

Unlike the electrochemical behaviors observed on CoO_xH_y, the cyclic voltammograms record on CoO_x under OER, GOR, and DOR conditions display no observable redox peaks in the lower potential region, as shown in Fig. 6a, despite that introduction of alcohol molecules (glycerol or DHA) induced clear cathodic shift of the onset potential. The lack of apparent redox peaks under all conditions suggests that CoO_x is rather stable under current oxidation environment, in agreement with previous reports [49]. In addition, SPECS experiments conducted on CoO_x electrode show that the current decay was capacitive in nature, further confirming the lack of redox-mediated events on CoO_x (Fig. 6b). Furthermore, in situ Raman spectra of CoO_x were also acquired. Four Raman-active phonon modes of cubic spinel Co_3O_4, E_g (484 cm^{-1}), $F_{2\,g}$ (524 cm^{-1}), $F_{2\,g}$ (621 cm^{-1}), and $A_{1\,g}$ (691 cm^{-1}) were observed under OCP condition. CoO_x displays no difference in Raman spectra from its OCP state throughout the applied potential window in presence of either glycerol (Fig. 6c) or DHA (Fig. 6d). These results indicate that CoO_x is electrochemically stable, with little Co^{3+} and Co^{4+} accumulation when glycerol or DHA was present. Similar conclusion can be made by ex situ XPS characterizations. Little changes were observed in the spectral profile of the high-resolution XPS spectra of Co 2p collected on CoO_x after electrocatalysis (Fig. S16a), while a slightly intensified peak of lattice oxygen in Co_3O_4 (O-O) was observed (Fig. S16b). Combined with the morphological characterization by SEM (Fig. S16c), our results suggest minor surface oxidation occurred on CoO_x after GOR, with good structural integrity maintained nonetheless.

In terms of efficiency and selectivity of electrochemical glycerol oxidation on CoO_x, DHA was the main component among the collected liquid oxidation products (Fig. S17a), similar to our previous study on Co-B_i [33] and reports by other groups [31,32]. The calculated Faradaic efficiencies for HPA, GA, FA, GLA, GLAD, and DHA were 3.1%, 4.0%, 5.7%, 5.0%, 5.1%, and 24.4%, respectively (Fig. S17b). The total Faradaic efficiency (~40%) and that for C_3 products are considerably lower than those on CoO_xH_y, consistent with the observation that considerable OER activity occurred on CoO_x under current experimental conditions (Fig. 6a and Fig. S18). In particular, the Faradaic efficiency of HPA on CoO_xH_y (43.2%) was 14 times of that on CoO_x (3.1%), and the production rate of HPA on CoO_xH_y (679.2 μmol min^{-1} m_{geo}^{-2}) is nearly 34-fold of that on CoO_x (20.55 μmol min^{-1} m_{geo}^{-2}). In terms of the solution product selectivity, DHA was the main solution products (over 60%), as shown in Fig. S19. The glycerol conversion can be inferred indirectly by calculating all the detected solution products using Eq. (11). For GOR performed on CoO_x at a constant potential of 1.56 V vs. RHE in 0.1 M borate buffer solution (pH 7.52) containing 0.05 M glycerol, the calculated glycerol conversion was 5.6% after 30 C were passed. Unlike that on CoO_xH_y, the total FE for solution products obtained on CoO_x electrodes remained near constant upon increasing the applied potential to 1.76 V (Fig. S20), with some of the generated DHA being further oxidized to HPA at high anodic potentials.

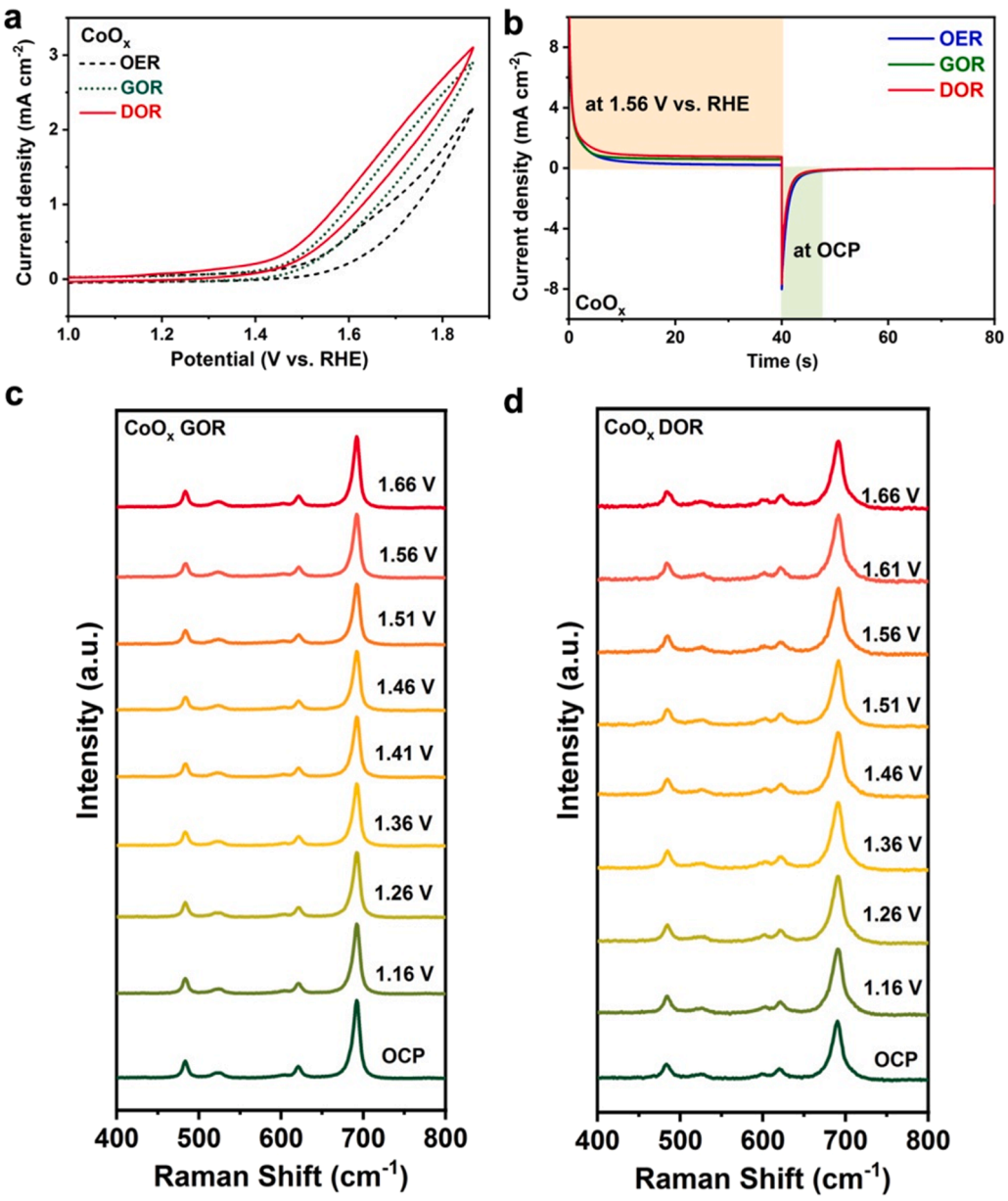

Fig. 6. (a) Cyclic voltammetry performed on CoO_x in 0.1 M borate buffer under OER, GOR, and DOR conditions, with the scan rate of 1 mV s^{-1}. (b) Step potential electrochemical spectroscopy measurements on CoO_x under different conditions. In situ Raman spectroscopy conducted on CoO_x electrodes at increasing applied potentials from OCP to 1.66 V in 0.1 M borate buffer solution with 0.05 M glycerol (c) or 0.05 M DHA (d).

3.6. *Proposed mechanism of HPA formation on CoO_xH_y*

By putting all the experimental pieces together, we tentatively propose the mechanism of selective glycerol oxidation toward HPA production on CoO_xH_y, as shown in Scheme 1. Despite lower ECSA compared to CoO_x, CoO_xH_y can generate large number of high-valent

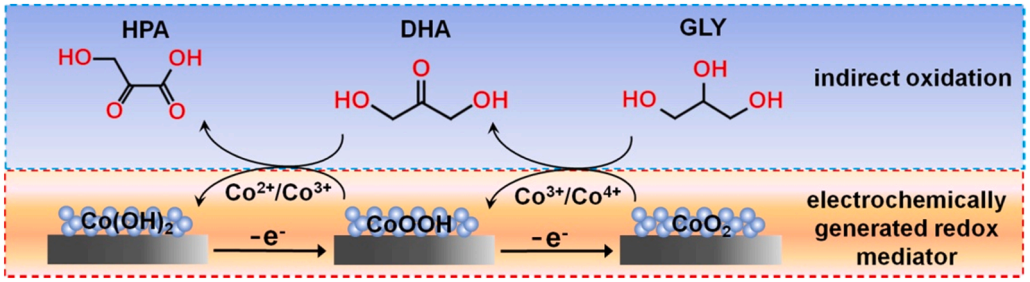

Scheme 1. Schematic illustration of the electrochemical glycerol oxidation toward HPA on CoO_xH_y electrodes through an indirect oxidation mechanism mediated by high-valent cobalt redox pairs.

cobalt species (Co^{3+} and Co^{4+}) under oxidative electrochemical conditions, and these in situ generated Co^{3+} and Co^{4+} then serve as the actual oxidation center for glycerol and DHA oxidation reactions. More specifically, Co^{3+}/Co^{4+} redox mediator induces indirect oxidation of glycerol to DHA, which is subsequently oxidized to HPA, also through an indirect route via Co^{2+}/Co^{3+} redox pair. This sequential oxidation step would deplete surface accumulation of high-valent cobalt species, as confirmed by cyclic voltammetry, SPECS, and in situ Raman results. In contrast, on the electrochemically stable CoO_x surface, the lack of in situ generated high-valent cobalt centers would prefer direct oxidation of glycerol to DHA, but not the more complex $4e^-$ oxidation from DHA to HPA. Therefore, it is the combined effect of the available number of high-valent cobalt sites and the redox property of Co^{3+} and Co^{4+} that determine the high activity and distinct selectivity toward HPA production on CoO_xH_y electrodes.

The critical role of high-valent cobalt redox mediators in enhancing glycerol oxidation and selectively producing HPA that we have revealed here, may provide a new perspective for low-cost transition metal electrocatalyst design and optimization, where electrochemical activity and selectively may be regulated toward specific value-added chemical generation.

4. Conclusion

In summary, by using substoichiometric cobalt (oxy)hydroxide CoO_xH_y as electrocatalyst, we have achieved selective electrochemical glycerol oxidation to hydroxypyruvic acid (HPA), an important C_3 chemical. The specific Faradaic efficiency for HPA production is over 40%, with an average production rate of 679.2 μmol min^{-1} $m_{geo}{}^{-2}$. By conducting cyclic voltammetry, step potential electrochemical spectroscopy, and in situ Raman spectroscopy measurements, we have revealed the important roles played by high-valent cobalt species in glycerol and DHA oxidation reactions. CoO_xH_y is discovered to produce Co^{2+}/Co^{3+} and Co^{3+}/Co^{4+} redox pairs efficiently under electrochemical conditions, which then mediate the dehydrogenation of glycerol to DHA and then to HPA. In comparison, the more electrochemically stable CoO_x produces DHA as the main product, with much lower activity and Faradaic efficiency. This work showcases the critical role of the high-valent transition metal redox mediator in enhancing the activity and regulating the product selectivity for electrochemical glycerol oxidation reactions, and may guide future electrocatalyst and system development for selective valorization of glycerol.

CRediT authorship contribution statement

Xin Huang: Conceptualization, Methodology, Investigation, Writing – original draft. **Yuyang Guo**: Methodology, Investigation. **Yu Zou**: Funding acquisition, Writing – review & editing. **Jiang Jiang**: Conceptualization, Supervision, Funding acquisition, Writing – review & editing, Project administration.

Declaration of Competing Interest

The authors declare that they have no known competing financial interests or personal relationships that could have appeared to influence the work reported in this paper.

Acknowledgments

This work was funded by National Natural Science Foundation of China (No. 21873113 and 21771190) and Youth Innovation Promotion Association of Chinese Academy of Sciences (2018358).

Appendix A. Supporting information

Supplementary data associated with this article can be found in the online version at doi:10.1016/j.apcatb.2022.121247.

References

[1] M.N. Bin Mohiddin, Y.H. Tan, Y.X. Seow, J. Kansedo, N.M. Mubarak, M. O. Abdullah, Y. San Chan, M. Khalid, Evaluation on feedstock, technologies, catalyst and reactor for sustainable biodiesel production: a review, J. Ind. Eng. Chem. 98 (2021) 60–81.
[2] M.R. Monteiro, C.L. Kugelmeier, R.S. Pinheiro, M.O. Batalha, A. da Silva César, Glycerol from biodiesel production: technological paths for sustainability, Renew. Sustain. Energy Rev. 88 (2018) 109–122.
[3] C.C. Chong, A. Aqsha, M. Ayoub, M. Sajid, A.Z. Abdullah, S. Yusup, B. Abdullah, A review over the role of catalysts for selective short-chain polyglycerol production from biodiesel derived waste glycerol, Environ. Technol. Innov. 19 (2020), 100859.
[4] M. Pagliaro, R. Ciriminna, H. Kimura, M. Rossi, C. Della Pina, From glycerol to value-added products, Angew. Chem. Int. Ed. 46 (2007) 4434–4440.
[5] A. Behr, J. Eilting, K. Irawadi, J. Leschinski, F. Lindner, Improved utilisation of renewable resources: new important derivatives of glycerol, Green Chem. 10 (2008) 13–30.
[6] C.H. Zhou, J.N. Beltramini, Y.X. Fan, G.Q. Lu, Chemoselective catalytic conversion of glycerol as a biorenewable source to valuable commodity chemicals, Chem. Soc. Rev. 37 (2008) 527–549.
[7] B. Katryniok, H. Kimura, E. Skrzyńska, J.-S. Girardon, P. Fongarland, M. Capron, R. Ducoulombier, N. Mimura, S. Paul, F. Dumeignil, Selective catalytic oxidation of glycerol: perspectives for high value chemicals, Green Chem. 13 (2011) 1960–1979.
[8] A. Talebian-Kiakalaieh, N.A.S. Amin, K. Rajaei, S. Tarighi, Oxidation of bio-renewable glycerol to value-added chemicals through catalytic and electrochemical processes, Appl. Energy 230 (2018) 1347–1379.
[9] G. Dodekatos, S. Schünemann, H. Tüysüz, Recent advances in thermo-, photo-, and electrocatalytic glycerol oxidation, ACS Catal. 8 (2018) 6301–6333.
[10] F.W.S. Lucas, R.G. Grim, S.A. Tacey, C.A. Downes, J. Hasse, A.M. Roman, C. A. Farberow, J.A. Schaidle, A. Holewinski, Electrochemical routes for the valorization of biomass-derived feedstocks: from chemistry to application, ACS Energy Lett. 6 (2021) 1205–1270.
[11] X. Deng, M. Li, Y. Fan, L. Wang, X.-Z. Fu, J.-L. Luo, Constructing multifunctional 'Nanoplatelet-on-Nanoarray' electrocatalyst with unprecedented activity towards novel selective organic oxidation reactions to boost hydrogen production, Appl. Catal. B 278 (2020), 119339.
[12] Y.X. Chen, A. Lavacchi, H.A. Miller, M. Bevilacqua, J. Filippi, M. Innocenti, A. Marchionni, W. Oberhauser, L. Wang, F. Vizza, Nanotechnology makes biomass electrolysis more energy efficient than water electrolysis, Nat. Commun. 5 (2014) 4036.
[13] S. Verma, S. Lu, P.J.A. Kenis, Co-electrolysis of CO_2 and glycerol as a pathway to carbon chemicals with improved technoeconomics due to low electricity consumption, Nat. Energy 4 (2019) 466–474.
[14] Y. Pei, Z. Pi, H. Zhong, J. Cheng, F. Jin, Glycerol oxidation-assisted electrochemical CO_2 reduction for the dual production of formate, J. Mater. Chem. A 10 (2022) 1309–1319.
[15] Y. Zhou, Y. Shen, J. Xi, Seed-mediated synthesis of PtxAuy@Ag electrocatalysts for the selective oxidation of glycerol, Appl. Catal. B 245 (2019) 604–612.
[16] T. Li, D.A. Harrington, An overview of glycerol electrooxidation mechanisms on Pt, Pd and Au, ChemSusChem 14 (2021) 1472–1495.
[17] B.J. Taitt, D.-H. Nam, K.-S. Choi, A comparative study of nickel, cobalt, and iron oxyhydroxide anodes for the electrochemical oxidation of 5-hydroxymethylfurfural to 2,5-furandicarboxylic acid, ACS Catal. 9 (2018) 660–670.
[18] H.-J. Qiu, G. Fang, J. Gao, Y. Wen, J. Lv, H. Li, G. Xie, X. Liu, S. Sun, Noble metal-free nanoporous high-entropy alloys as highly efficient electrocatalysts for oxygen evolution reaction, ACS Mater. Lett. 1 (2019) 526–533.
[19] S. Anantharaj, V. Aravindan, Developments and perspectives in 3d transition-metal-based electrocatalysts for neutral and near-neutral water electrolysis, Adv. Energy Mater. 10 (2020), 1902666.
[20] L. Lv, Z. Yang, K. Chen, C. Wang, Y. Xiong, 2D layered double hydroxides for oxygen evolution reaction: from fundamental design to application, Adv. Energy Mater. 9 (2019), 1803358.
[21] M.S.E. Houache, R. Safari, U.O. Nwabara, T. Rafaïdeen, G.A. Botton, P.J.A. Kenis, S. Baranton, C. Coutanceau, E.A. Baranova, Selective electrooxidation of glycerol to formic acid over carbon supported Ni1–xMx (M = Bi, Pd, and Au) nanocatalysts and coelectrolysis of CO_2, ACS Appl. Energy Mater. 3 (2020) 8725–8738.
[22] X. Han, H. Sheng, C. Yu, T.W. Walker, G.W. Huber, J. Qiu, S. Jin, Electrocatalytic oxidation of glycerol to formic acid by CuCo2O4 spinel oxide nanostructure catalysts, ACS Catal. 10 (2020) 6741–6752.
[23] Y. Li, X. Wei, L. Chen, J. Shi, M. He, Nickel-molybdenum nitride nanoplate electrocatalysts for concurrent electrolytic hydrogen and formate productions, Nat. Commun. 10 (2019) 5335.
[24] M.S.E. Houache, K. Hughes, E.A. Baranova, Study on catalyst selection for electrochemical valorization of glycerol, Sustain. Energy Fuels 3 (2019) 1892–1915.
[25] M.S. Ahmad, M.H. Ab Rahim, T.M. Alqahtani, T. Witoon, J.W. Lim, C.K. Cheng, A review on advances in green treatment of glycerol waste with a focus on electro-oxidation pathway, Chemosphere 276 (2021), 130128.
[26] M. Guschakowski, U. Schroder, Direct and indirect electrooxidation of glycerol to value-added products, ChemSusChem 14 (2021) 5216–5225.

[27] M. Simoes, S. Baranton, C. Coutanceau, Electrochemical valorisation of glycerol, ChemSusChem 5 (2012) 2106–2124.
[28] L. Fan, B. Liu, X. Liu, N. Senthilkumar, G. Wang, Z. Wen, Recent progress in electrocatalytic glycerol oxidation, Energy Technol. 9 (2020), 2000804.
[29] C. Coutanceau, S. Baranton, R.S.B. Kouame, Selective electrooxidation of glycerol into value-added chemicals: a short overview, Front. Chem. 7 (2019) 100.
[30] P.A. Alaba, C.S. Lee, F. Abnisa, M.K. Aroua, P. Cognet, Y. Pérès, W.M.A. Wan Daud, A review of recent progress on electrocatalysts toward efficient glycerol electrooxidation, Rev. Chem. Eng. (2020), 20190013.
[31] C. Liu, M. Hirohara, T. Maekawa, R. Chang, T. Hayashi, C.-Y. Chiang, Selective electro-oxidation of glycerol to dihydroxyacetone by a non-precious electrocatalyst – CuO, Appl. Catal. B 265 (2020), 118543.
[32] T.-G. Vo, P.-Y. Ho, C.-Y. Chiang, Operando mechanistic studies of selective oxidation of glycerol to dihydroxyacetone over amorphous cobalt oxide, Appl. Catal. B 300 (2022), 120723.
[33] X. Huang, Y. Zou, J. Jiang, Electrochemical oxidation of glycerol to dihydroxyacetone in borate buffer: enhancing activity and selectivity by borate–polyol coordination chemistry, ACS Sustain. Chem. Eng. 9 (2021) 14470–14479.
[34] H.Y. Wang, S.F. Hung, H.Y. Chen, T.S. Chan, H.M. Chen, B. Liu, In operando identification of geometrical-site-dependent water oxidation activity of spinel Co3O4, J. Am. Chem. Soc. 138 (2016) 36–39.
[35] A. Bergmann, T.E. Jones, E. Martinez Moreno, D. Teschner, P. Chernev, M. Gliech, T. Reier, H. Dau, P. Strasser, Unified structural motifs of the catalytically active state of Co(oxyhydr)oxides during the electrochemical oxygen evolution reaction, Nat. Catal. 1 (2018) 711–719.
[36] A. Moysiadou, S. Lee, C.S. Hsu, H.M. Chen, X. Hu, Mechanism of oxygen evolution catalyzed by cobalt oxyhydroxide: cobalt superoxide species as a key intermediate and dioxygen release as a rate-determining step, J. Am. Chem. Soc. 142 (2020) 11901–11914.
[37] J. Huang, H. Sheng, R.D. Ross, J. Han, X. Wang, B. Song, S. Jin, Modifying redox properties and local bonding of Co3O4 by CeO2 enhances oxygen evolution catalysis in acid, Nat. Commun. 12 (2021) 3036.
[38] X. Deng, G.Y. Xu, Y.J. Zhang, L. Wang, J. Zhang, J.F. Li, X.Z. Fu, J.L. Luo, Understanding the roles of electrogenerated Co(3+) and Co(4+) in selectivity-tuned 5-hydroxymethylfurfural oxidation, Angew. Chem. Int. Ed. 60 (2021) 20535–20542.
[39] B. Mondal, N. Karjule, C. Singh, R. Shimoni, M. Volokh, I. Hod, M. Shalom, Unraveling the mechanisms of electrocatalytic oxygenation and dehydrogenation of organic molecules to value-added chemicals over a Ni–Fe oxide catalyst, Adv. Energy Mater. 11 (2021), 2101858.
[40] Y. Xie, Z. Zhou, N. Yang, G. Zhao, An overall reaction integrated with highly selective oxidation of 5–hydroxymethylfurfural and efficient hydrogen evolution, Adv. Funct. Mater. 31 (2021), 2102886.
[41] P. Zhang, X. Sheng, X. Chen, Z. Fang, J. Jiang, M. Wang, F. Li, L. Fan, Y. Ren, B. Zhang, B.J.J. Timmer, M.S.G. Ahlquist, L. Sun, Paired electrocatalytic oxygenation and hydrogenation of organic substrates with water as the oxygen and hydrogen source, Angew. Chem. Int. Ed. 58 (2019) 9155–9159.
[42] B. Zhou, Y. Li, Y. Zou, W. Chen, W. Zhou, M. Song, Y. Wu, Y. Lu, J. Liu, Y. Wang, S. Wang, Platinum modulates redox properties and 5-hydroxymethylfurfural adsorption kinetics of Ni(OH)2 for biomass upgrading, Angew. Chem. Int. Ed. 60 (2021) 22908–22914.
[43] M.T. Bender, Y.C. Lam, S. Hammes-Schiffer, K.S. Choi, Unraveling two pathways for electrochemical alcohol and aldehyde oxidation on NiOOH, J. Am. Chem. Soc. 142 (2020) 21538–21547.
[44] Z. Song, X. Han, Y. Deng, N. Zhao, W. Hu, C. Zhong, Clarifying the controversial catalytic performance of Co(OH)2 and Co3O4 for oxygen reduction/evolution reactions toward efficient Zn–Air batteries, ACS Appl. Mater. Interfaces 9 (2017) 22694–22703.
[45] J. Yang, H. Liu, W.N. Martens, R.L. Frost, Synthesis and characterization of cobalt hydroxide, cobalt oxyhydroxide, and cobalt oxide nanodiscs, J. Phys. Chem. C 114 (2010) 111–119.
[46] N.P. Dileep, T.V. Vineesh, P.V. Sarma, M.V. Chalil, C.S. Prasad, M.M. Shaijumon, Electrochemically exfoliated β-Co(OH)2 nanostructures for enhanced oxygen evolution electrocatalysis, ACS Appl. Energy Mater. 3 (2020) 1461–1467.
[47] M.C. Biesinger, B.P. Payne, A.P. Grosvenor, L.W.M. Lau, A.R. Gerson, R.S.C. Smart, Resolving surface chemical states in XPS analysis of first row transition metals, oxides and hydroxides: Cr, Mn, Fe, Co and Ni, Appl. Surf. Sci. 257 (2011) 2717–2730.
[48] M. Fleischmann, K. Korinek, D. Pletcher, The kinetics and mechanism of the oxidation of amines and alcohols at oxide-covered nickel, silver, copper, and cobalt electrodes, J. Chem. Soc. Perkin Trans. 2 (1972) 1396–1403.
[49] H.Y. Wang, S.F. Hung, Y.Y. Hsu, L. Zhang, J. Miao, T.S. Chan, Q. Xiong, B. Liu, In situ spectroscopic identification of mu-OO bridging on spinel Co3O4 water oxidation electrocatalyst, J. Phys. Chem. Lett. 7 (2016) 4847–4853.
[50] H. Lindström, S. Södergren, A. Solbrand, H. Rensmo, J. Hjelm, A. Hagfeldt, S.-E. Lindquist, Li+ ion insertion in TiO2 (Anatase). 2. Voltammetry on nanoporous films, J. Phys. Chem. B 101 (1997) 7717–7722.
[51] M.F. Dupont, S.W. Donne, Separating Faradaic and non-Faradaic charge storage contributions in activated carbon electrochemical capacitors using electrochemical methods I. Step potential electrochemical spectroscopy, J. Electrochem. Soc. 162 (2015) A1246–A1254.
[52] T. Nishi, H. Nakai, A. Kita, Visualization of the state-of-charge distribution in a LiCoO2 cathode by in situ Raman imaging, J. Electrochem. Soc. 160 (2013) A1785–A1788.
[53] Z. Chen, L. Cai, X. Yang, C. Kronawitter, L. Guo, S. Shen, B.E. Koel, Reversible structural evolution of NiCoOxHy during the oxygen evolution reaction and identification of the catalytically active phase, ACS Catal. 8 (2018) 1238–1247.
[54] Y.-C. Liu, J.A. Koza, J.A. Switzer, Conversion of electrodeposited Co(OH)2 to CoOOH and Co3O4, and comparison of their catalytic activity for the oxygen evolution reaction, Electrochim. Acta 140 (2014) 359–365.